Multiresolution spline warping for EPI registration

Jan Kybic, Philippe Thévenaz, and Michael Unser

Biomedical Imaging Group, DMT/IOA
Swiss Federal Institute of Technology Lausanne
CH-1015 Lausanne EPFL, Switzerland

ABSTRACT

Registration of images subject to non-linear warping has numerous practical applications. We present an algorithm based on double multiresolution structure of warp and image spaces. Tuning a so-called scale parameter controls the coarseness of the grid by which the deformation is described and also the amount of implicit regularization. The application of our algorithm deals with undoing unidirectional non-linear geometrical distortion of echo-planar images (EPI) caused by local magnetic field inhomogeneities induced mainly by the subject presence. The unwarping is based on registering the EPI images with corresponding undistorted anatomical MRI images.

We present evaluation of our method using a wavelet-based random Sobolev-type deformation generator as well as other experimental examples.

Keywords: registration, warping, splines, EPI, geometrical distortion, multiresolution

1. INTRODUCTION

In the biomedical domain, image registration can be used for a variety of tasks; for example, motion analysis, inter-subject, intra-subject, or inter-modality matching, stereotactic normalization, and distortion compensation. See,[1] for a more complete list. This article deals with the development of a specific image registration algorithm for distortion compensation of EPI images.

1.1. Unwarping of EPI images

Echo planar imaging (EPI)[2] is a fast magnetic resonance imaging (MRI) technique. It is used mainly for functional imaging (fMRI), the *in vivo* non-invasive study of the temporal, spatial and behavioral dependencies of brain activities. In contrast to conventional MRI, where the number of excitations per slice is equal to the number of scan lines, in EPI the magnetic field gradients simultaneously encode two coordinates during one excitation. As one of the gradients (the so-called phase-encoding gradient) is several orders of magnitude weaker than the other, the inhomogeneous magnetic field will manifest itself mainly as a geometrical distortion of the 2D slice image along the direction of this gradient. The stronger gradient being less affected, the distortion is essentially unidirectional.

The deformation makes direct use of fMRI images difficult in applications like stereotactic surgery and hinders the performance of others, like localization of zones of activation.

1.2. Distortion correction techniques

Some existing unwarping techniques modify the acquisition procedure,[3–5] which is not always practical. Others use a two-step procedure[3,6] consisting of correcting the deformation with a help of a deformation map previously obtained using a phantom. The major drawback of these methods is that it is difficult to make a phantom which would exactly duplicate the biological system being imaged.

We propose a third approach which, to the best of our knowledge, has never been applied to this particular problem. It consists of registering the distorted EPI image with a corresponding geometrically correct anatomical MRI image. In this way, we can recover the deformation from a single EPI slice obtained by an unaltered, standard procedure. Once the deformation is known, the observed EPI image can be warped back to undo the distortion.

Correspondence: email: Jan.Kybic@epfl.ch

1.3. Registration algorithms

There are many image registration algorithms based on different techniques. Each uses its particular hypotheses and its particular tradeoffs, tuned to give the best results for a given application. See[7] for a general survey of existing linear, as well as non-linear, image registration algorithms. We shall categorize registration algorithms according to the *warp* space used.

At one end of the scale we have *non-parametric, local methods*. These methods are formulated either as *variational*, defining a scalar criterion to minimize, or (more generally) using PDEs. The continuously defined correspondence function minimizing a given criterion, resp. solving a given PDE, is sought for in a very large and unrestrictive functional space, e.g., the Sobolev space W_2^2. The essence of these methods is *entirely in the criterion*, resp. PDE. The PDE come from the optical flow approach (gradient methods),[8] viscous fluid model,[9–11] elastic deformations with physical analogs[12,13] or without.[14] Some deformation fields can also be modeled as potential fields.[15]

At the other end, we have *parametric, global methods* that describe the correspondence function using a global model with a relatively small number of parameters.[16] The model mostly consists of expressing the warping function in a linear,[17] global polynomial,[18] or harmonic basis.[19] For these methods, the deformation model, which corresponds to a specific warp space, is as important as the criterion being minimized.

None of the existing techniques is directly applicable for our problem because of its specific features, mainly the unidirectionality of the deformation. We have therefore developed our own algorithm based on a warp model situated between the above-mentioned local and global methods, combining the advantages of both.

2. PROPOSED ALGORITHM

The image registration problem can be defined as follows: Given two images f_1, f_2 representing the same object, the image registration task seeks to identify geometric correspondences between homologous features in both images. Specifically, we want to find a *correspondence function* (also called deformation function or deformation field) $g(x_1) = x_2$, where x_1, x_2 are coordinates of matching objects in images f_1, f_2. Here, we intend to concentrate on a *non-linear* registration (also called *elastic matching*), characterized by the non-linearity of the function g.

Warping an image f_2 by a deformation g, we obtain a warped version $g \circ f_2$, where $(g \circ f_2)(x) = f_2(g(x))$. If the warping g is correct (that is, close to the true deformation g_T), the image $g \circ f_2$ should be similar to the image f_1. This leads to a broad class of algorithms that search an optimal g minimizing a dissimilarity between a warped version of a *test image* $(g \circ f_2)$ and a reference image (f_1). Symbolically,

$$g_J = \arg\min_{g \in V} \underbrace{\mathcal{L}(g \circ f_2, f_1)}_{J} \tag{1}$$

where $\mathcal{L}$ is a dissimilarity measure, J the value of the criterion, V is a *warp space*, and g_J is the optimal warping function in the sense of this criterion.

2.1. Warp space

In practice, the function g is always specified by a finite number of (real scalar) parameters $\{c_k\}_{k=1}^{L}$ by means of a model Φ

$$g(x) = \Phi(x; \{c_k\}) \tag{2}$$

All functions representable by this model form a space (not necessarily a vector space, though)

$$V = \left\{ \Phi(x; \{c_k\});\ \{c_k\} \in Q \subseteq \mathbb{R}^L \right\} \tag{3}$$

where Q is the set of all admissible parameter values.

Generally, the true warping g_T will not belong to V. The best approximation of g_T from V (in the sense of some norm $\mathcal{M}$) is called a *projection* and denoted $P_V g_T = g_V$. The error we make is $\varpi_{\min} = \|g_V - g_T\|_{\mathcal{M}}$. Its value is the lower bound for the overall registration error; we want it to be as small as possible for reasonable deformations g_T.

2.2. Optimization algorithm

The optimal g_J from V minimizing the criterion J from (1) is found by iterative multidimensional non-linear optimization with respect to parameters c_k. We normally use a regularized version of the Newton method,[17, 20] inspired by the Marquardt-Levenberg algorithm. The algorithm uses the first two derivatives of the criterion E with respect to c_k, $\nabla_c E$ and $\nabla_c^2 E$. The particularity of this algorithm is that it smoothly varies between the gradient-descent and the Newton approach, which gives it robustness and quadratic convergence near the optimum.

2.3. Multiresolution

We will parametrize Φ by a scale parameter h, creating a coarse-to-fine sequence of models $\Phi_{h_1}, \Phi_{h_2}, \ldots, \Phi_{h_m}$ for $h_1 > h_2 > \ldots > h_m$ so that $V_{h_1} \subseteq V_{h_2} \subseteq \ldots \subseteq V_{h_m}$. This implies $\varpi_{h_1} \geq \varpi_{h_2} \geq \ldots \geq \varpi_{h_m}$; that is, the representation error decreases with h. By construction of the models, we will want the number of parameters to decrease as h increases; i.e., $L_{h_1} \leq L_{h_2} \leq \ldots L_{h_m}$. We call the series of models with their associated parameters a *model pyramid*.

Similarly, we construct *image pyramids* for both images f_1, f_2.

2.4. Multiresolution optimization

The robustness and efficiency of our algorithm is significantly improved by the multiresolution approach. The optimization task is first solved at the coarsest level of the pyramid. Then, the results are propagated to the next finer level and used as a starting guess for solving the task at that level. This procedure is iterated until the finest level is reached.

Since we have two separate pyramids for model and images, we combine the two multiresolution strategies by alternating scale changes for the model and image.

2.5. Warp space model

The warp space, and consequently also the model generating this space, should satisfy the following requirements:

(a) *Good approximation properties*—we should be able to approximate a realistic warping function g by g_V from V with a small error. Ideally, affine deformations (which occur frequently) should be representable exactly.

(b) *Speed*—evaluation of g_V is a fundamental operation in the registration process; it is therefore important to accelerate it. In the linear generator case, this corresponds to short and fast-to-evaluate generating functions.

(c) *Plausibility*—the warping space should contain only deformations which are plausible for a given application. In this way, we limit the quantity of candidate solutions to be searched, which speeds up and stabilizes the registration. Furthermore, we alleviate or remove the need for explicit regularization.

(d) *Simplicity*—to get a fast algorithm it is paramount to minimize the number of parameters and thus the dimensionality of this space. Clearly, (with the same amount of information available) as the number of parameters to estimate increases, the task gets more difficult and the results become less accurate and less robust. It is also highly advantageous that the dependence of g_V on c_k be simple (ideally linear), as this increases the chance that the information gathered locally will be reasonably accurate in some extended neighborhood.

We express the warping function as a linear combination of uniformly spaced translates of a generating function φ, where we take φ to be a B-spline β_r of degree r. (In multiple dimensions, we use a tensor product of B-splines.)

$$g(x) = \sum_{k \in K} c_k \, \varphi(x/h - k) \tag{4}$$

A good choice seems to be $r = 3$. This way, we obtain a model that fulfills well the requirements above. See Appendix for a definition of a B-spline.

2.6. Image interpolation model

An *image interpolation* model is needed to calculate the warped image $g \circ f_2$ for the criterion evaluation. We need to get a continuous form of a discrete image. Because of their good approximation properties, simple analytic form and effective algorithms available, we use B-splines here too.

$$ {}^{c}f(x) = \sum_i b_i \, \beta(x - i) \quad \text{where} \quad {}^{c}f(i) = f(i), \, \forall \, i \in I \tag{5} $$

The coefficients b_i can be obtained prior to registration by an efficient filtering algorithm,[21] which incurs negligible overhead. For the filtering, we are using mirror boundary conditions on the the image. In this way we have the same number of coefficients b_i as pixels in the original image.

2.7. Data criterion

A reasonable way to measure the discrepancy between two images is the *sum of squared differences* (SSD) criterion

$$ E = \sum_{i \in I} \left(f_2(g(i)) - f_1(i) \right)^2 \tag{6} $$

where the sum is over all pixels in the image. To minimize this criterion is equivalent to calculating the maximum likelihood estimate of the unknown parameters, assuming that the image f_1 is a geometrically distorted version of the image f_2, along with additive i.i.d. Gaussian noise. To make the test and reference images more similar, we apply a preprocessing step to both images that consists of high-pass filtering and histogram equalization.

3. EXPERIMENTS

The performance of our algorithm was tested on several hundreds of images. In addition, thirty image pairs were manually registered by three different people, including one experienced practitioner, and the results compared with the automatic method. For the manual registration, we use the standard thin-plate spline method.[22–24]

3.1. Deformation generator

To test our algorithm, we have implemented a wavelet-based deformation generator. We want to generate a random Sobolev-type deformation—a deformation lying in a prescribed Sobolev space W_2^r. The higher the r, the more regular are the functions from W_2^r. Wavelets are known to be good bases for functions lying in Sobolev spaces, and the decay of wavelet coefficients across scales is directly related to a Sobolev-type regularity. Let $\theta_{j,k}$ denote the coefficients of a wavelet expansion*

$$ g - g_I = \sum_{j,k} \theta_{j,k} \, \psi(x 2^j - k) \tag{7} $$

where g_I is an identity transform, and ψ is an orthogonal wavelet. Then $g - g_I$ belongs to a Sobolev space W_2^r if and only if

$$ \sum_{j,k} 2^{2jr} \left| \theta_{j,k} \right|^2 < \infty \tag{8} $$

provided that the regularity of ψ is greater than r.[25] It follows that for (8) to hold, the necessary condition is

$$ \exists \, C \in \mathbb{R}; \left| \theta_{j,k} \right|^2 < C \, \xi^j \quad \text{with} \quad \xi = 2^{-2r} \tag{9} $$

Practically, we shall generate our deformations using zero-mean, normally distributed coefficients with variance

$$ \mathbf{E} \left\{ \theta_{j,k}^2 \right\} = \sigma_0^2 \, \xi^j \tag{10} $$

where σ_0^2 governs the total energy of the deformation. Note that the generated displacements are white noise for $r = 0$ and become progressively smoother as r increases; their regularity converge to that of the generating wavelet ψ for

*For brevity, we deal here with the unidimensional case only.

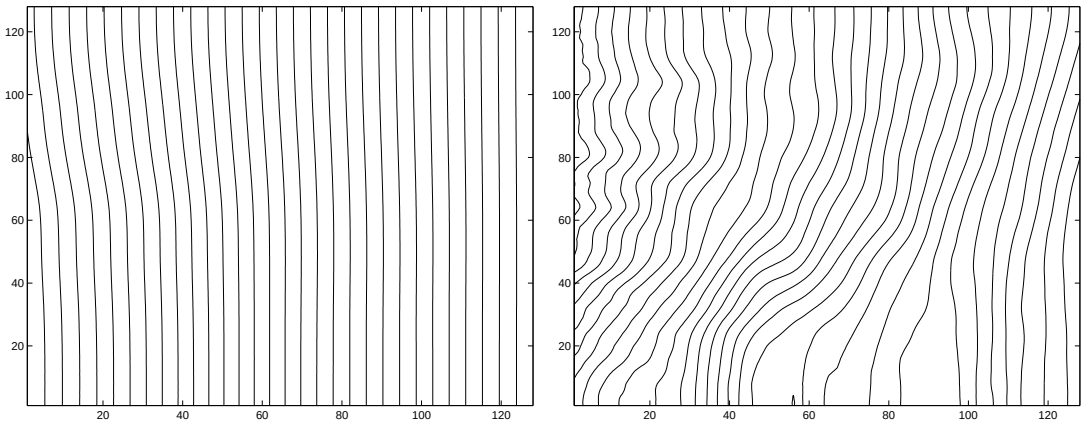

Figure 1. Example of a unidirectional bi-variate hierarchical deformation, presented as contour plots. On the left, $r = 1.6$, on the right, $r = 0.6$, in both cases $\sigma = 10$.

$r \to \infty$. For moderate to large r, we get a *hierarchical* warping: a deformation comprising displacements at several scale levels with gradually decreasing amplitudes, from important coarse-level deformations towards progressively smaller finer-level details. The algorithm should work well for such deformations, which are compatible with the multiresolution strategy.

Finally, the deformation can be projected onto V_h if needed. Typically, we use Battle-Lemarié wavelets of order 4, $\sigma_0 = 5$ and $r = 0.5 \sim 1.6$, depending of what aspect of the algorithm we want to highlight. For some experiments, we also add a random affine component. Examples of generated deformations are shown in Figure 1.

3.2. Controlled environment

Figure 2 shows results of a controlled experiment. The reference (f_1) and test (f_2) images are identical except for a known transformation. We use a random Sobolev deformation with $\sigma = 5$ and $r = 1.6$. We measure the sum of square differences (SSD) and the warping index (the average difference between the calculated and the true warping in the region of interest) after registration as a function of the knot spacing h and the warp spline degree n.

We show how both error measures (E and ϖ) decrease as the knot spacing h decreases. Moreover, we demonstrate the advantage of using cubic splines to represent the warping, as opposed to linear and quadratic ones. The minimum achievable error $\varpi_{\min}$ is shown by the dotted line for the cubic case and marked *optimal*. Note that, except for the smallest knot spacing h, the warping index $\varpi_{\min}$ is very close to the calculated values.

3.3. Noisy case

Figure 3 demonstrates the dependence of the registration accuracy on the signal-to-noise ratio. For this series of experiments, the test images are obtained from a known transformation of a reference image with various levels of white Gaussian noise added. Here, we use a random Sobolev deformation with $\sigma = 5$ and $r = 1.16$ projected into the warp space with $h = 32$. We observe that the degradation of the algorithm's performance by noise is graceful for $\mathrm{SNR} > 10\,\mathrm{dB}$.

3.4. Real images

Figure 4 shows a typical pair of corresponding anatomical and EPI images, along with superimposed contours of the anatomical image before and after manual and automatic registration. It illustrates that the automatic procedure leads to subjectively comparable or better results than the manual one.

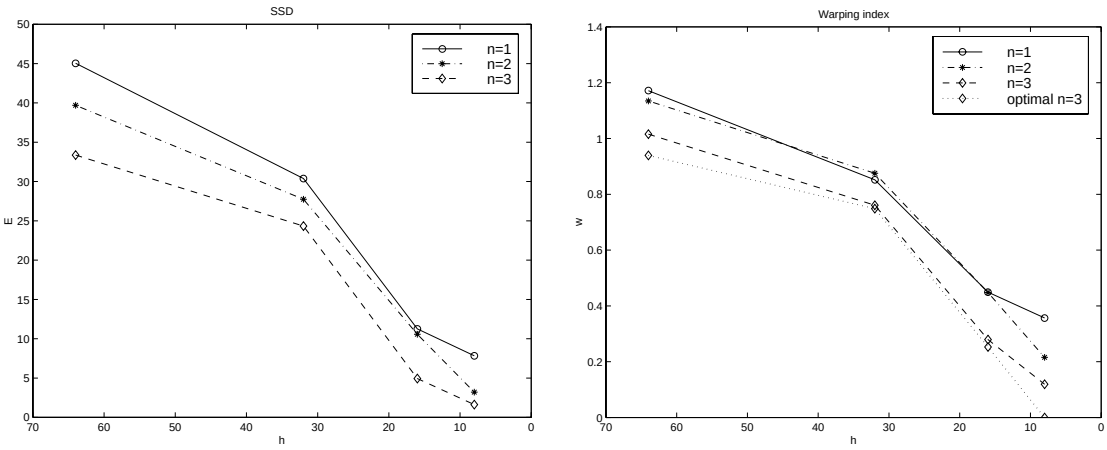

Figure 2. The quality of the registration as a function of the warp spline degree and the knot spacing. The initial values ranges (prior to the registration) were $E = 150$ and $\varpi = 3.5$. Each point shown is an average of thirty experiments.

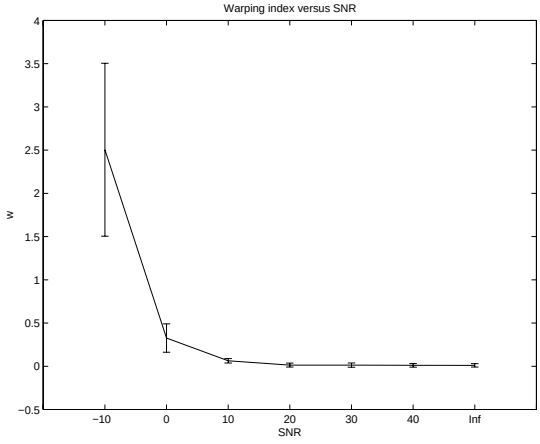

Figure 3. The quality of the registration as a function of the SNR in dB. $h = 32$, $\varpi_{\text{before}} = 3.34$. The error bars mark one standard deviation.

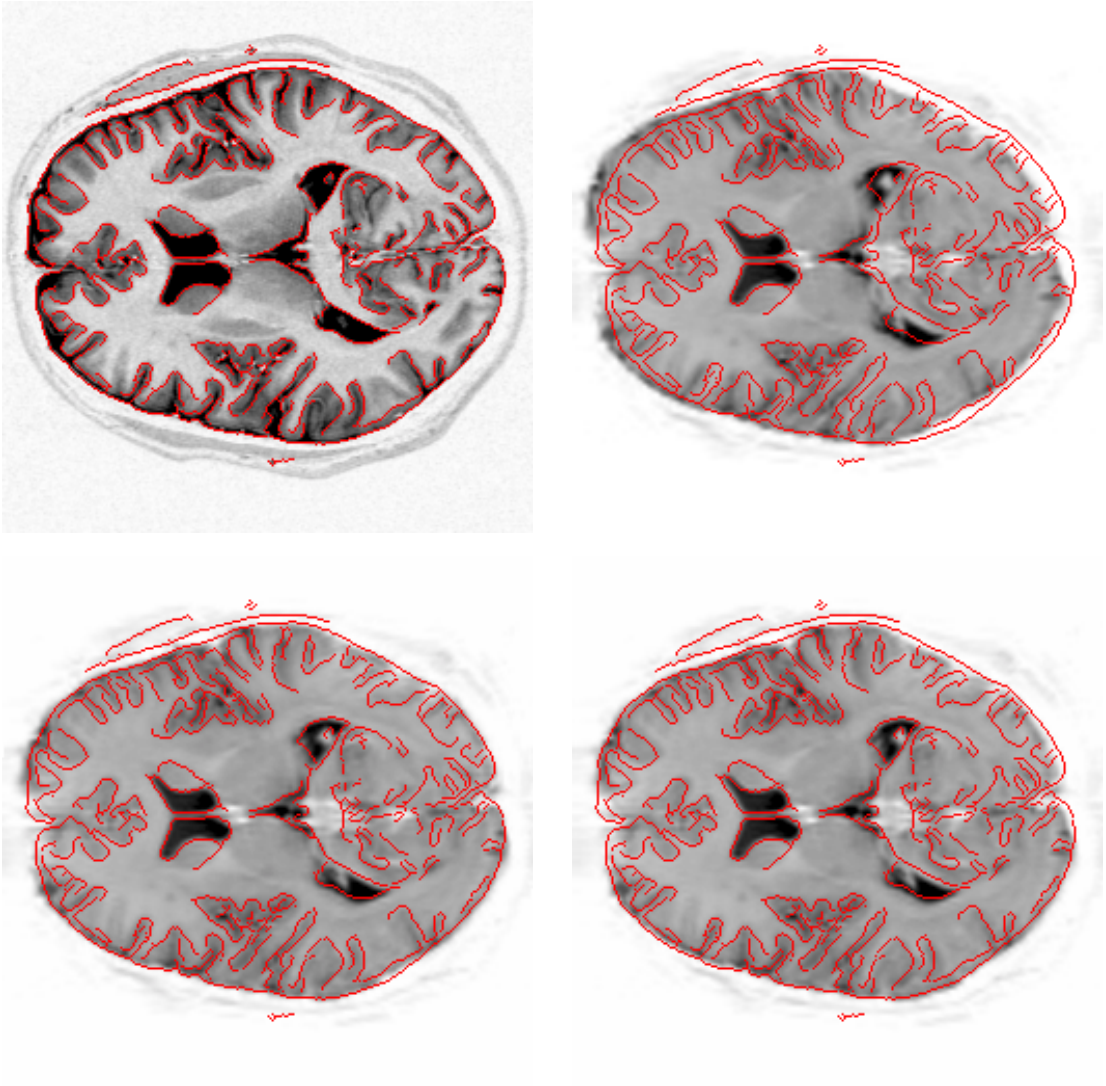

Figure 4. Anatomical (top-left) and EPI (top-right) images before registration, with superimposed contours from the anatomical images. EPI images after automatic (bottom-left) and manual (bottom-right) registration.

4. CONCLUSION

We have suggested a new approach for undoing non-linear deformation in EPI images by registering them with corresponding geometrically correct anatomical MRI images. We have developed a fully automatic image registration algorithm specialized for this task.[†]

The novelty of our registration algorithm stems from a high-order spline model for the warping. This model has good approximation properties and lends itself well to a multiresolution approach, while permitting an efficient implementation. We have also benefited from a spline model for the image being warped, leading to a second dimension of the multiresolution strategy and yielding additional computational savings. Finally, we have replaced the customary regularization criterion by a scale parameter of the search space.

ACKNOWLEDGMENTS

We would like to thank Arto Nirkko for bringing the EPI distortion problem to our attention, for explaining to us the intricacies of fMRI, and for providing us with data.

A B-spline β_r of degree r is recursively defined as

$$\beta_r = \beta_{r-1} * \beta_0 \quad \text{for } r > 0$$
$$\beta_0(x) = \begin{cases} 1 & \text{if } x \in (-\frac{1}{2}, \frac{1}{2}) \\ 0 & \text{otherwise} \end{cases}$$

B-splines, as defined above, are piecewise polynomial of degree r, have a compact support $(-r/2 - 1/2, r/2 + 1/2)$, are symmetric, and $(r-1)$-times continuously differentiable everywhere. As an example, we give the explicit form of the cubic B-spline, which is the function that we have found to be the most useful for our purpose.

$$\beta_3(x) = \begin{cases} 2/3 - (1 - |x|/2)x^2 & \text{if } 0 < |x| \leq 1 \\ (2 - |x|)^3/6 & \text{if } 1 < |x| < 2 \\ 0 & \text{otherwise} \end{cases} \tag{11}$$

REFERENCES

1. H. Lester and S. R. Arridge, "A survey of hierarchical non-linear medical image registration," *Pattern Recognition*, vol. 32, p. 129, Jan. 1999.
2. Z.-H. Cho, J. P. Jones, and M. Singh, *Foundations of Medical Imaging*. John Wiley & Sons, 1993.
3. H. Chang and J. M. Fitzpatrick, "A technique for accurate magnetic resonance imaging in the presence of field inhomogeneities," *IEEE Transactions on Medical Imaging*, vol. 11, pp. 319–329, 1992.
4. A. L. Alexander, J. S. Tsuruda, and D. L. Parker, "Elimination of Eddy current artifacts in diffusion-weighted echo-planar images: The use of bipolar gradients," *Magnetic Resonance in Medicine*, vol. 38, no. 6, pp. 1016–1021, 1997.
5. X. Wan, G. T. Gullberg, D. L. Parker, and G. L. Zeng, "Reduction of geometric and intensity distortions in echo-planar imaging using a multireference scan," *Magnetic Resonance in Medicine*, vol. 37, no. 6, pp. 932–942, 1997.
6. P. Jezzard and R. S. Balaban, "Correction for geometric distortion in echo planar images from B_0 field variations," *Magnetic Resonance in Medicine*, no. 34, pp. 65–73, 1995.
7. L. Brown, "A survey of image registration techniques," *ACM Computing Surveys*, vol. 24, pp. 326–376, Dec. 1992.
8. B. Horn and B. Schunck, "Determining optical flow," *Artificial Inteligence*, vol. 17, pp. 185–203, 1981.
9. G. Christensen, *Deformable Shape Models for Anatomy*. PhD thesis, Washington University, Saint Louis, Mississippi, 1994.

[†]An online demonstration of our algorithm is available on our WEB page `http://bigwww.epfl.ch`.

10. G. Christensen, S. Joshi, and M. Miller, "Volumetric transformation of brain anatomy," *IEEE Transactions on Medical Imaging*, vol. 16, Dec. 1997.
11. M. Bro-Nielsen and C. Gramkow, "Fast fluid registration of medical images," in *Visualization in Biomedical Computing* (K. H. Höhne and R. Kikinis, eds.), pp. 267–276, Springer-Verlag, 1996.
12. R. Bajcsy and S. Kovačič, "Multiresolution elastic matching," *Computer Vision, Graphics, and Image Processing*, vol. 46, pp. 1–21, 1989.
13. D. V. Iosifescu, M. E. Shenton, S. K. Warfield, R. Kikinis, J. Dengler, F. A. Jolesz, and R. W. McCarley, "An automated registration algorithm for measuring MRI subcortical brain structures," *Neuroimage*, no. 6, pp. 14–25, 1997.
14. Y. Tai, K. Lin, C. Hoh, S. Huang, and E. Hoffman, "Utilization of 3D elastic transformations in the registration of chest X-ray CT and whole body PET," *IEEE Transactions on Nuclear Science*, vol. 44, Aug. 1997.
15. T. Schormann, S. Henn, and K. Zilles, "A new approach to fast elastic alignment with applications to human brains," in *Visualization in Biomedical Computing* (K. H. Höhne and R. Kikinis, eds.), Springer-Verlag, 1996.
16. J. Bergen, P. Anandan, K. Hanna, and R. Hingorani, "Hierarchical model-based motion estimation," in *Second European Conference on Computer Vision (ECCV'92)*, pp. 237–252, Springer-Verlag, 1992.
17. P. Thévenaz, U. E. Ruttimann, and M. Unser, "A pyramid approach to subpixel registration based on intensity," *IEEE Transactions on Image Processing*, vol. 7, pp. 1–15, Jan. 1998.
18. N. Sicotte, R. Woods, and J. Mazziotta, "Automated image registration using a 105 parameter non-linear model," *Neuroimage*, vol. 3, June 1996. Second International Conference on Functional Mapping of the Human Brain.
19. S. Kiebel, J. Ashburner, J. Poline, and K. Friston, "MRI and PET coregistration—a cross validation of statistical parametric mapping and automated image registration," *Neuroimage*, no. 5, 1997.
20. W. H. Press, S. A. Teukolsky, W. T. Vetterling, and B. P. Flannery, *Numerical Recipes in C.* Cambridge University Press, second ed., 1992.
21. M. Unser, A. Aldroubi, and M. Eden, "B-spline signal processing: Part II—efficient design and applications," *IEEE Transactions on Signal Processing*, vol. 41, pp. 834–848, Feb. 1993.
22. K. Rohr, H. S. Stiehl, R. Sprengel, W. Beil, T. M. Buzug, J. Weese, and M. H. Kuhn, "Point-based elastic registration of medical image data using approximating thin-plate splines," in *Visualization in Biomedical Computing* (K. H. Höhne and R. Kikinis, eds.), pp. 297–306, Springer-Verlag, 1996.
23. J. Duchon, "Splines minimizing rotation-invariant semi-norms in Sobolev spaces," in *Constructive Theory of Functions of Several Variables* (W. Schempp and K. Zeller, eds.), (Berlin), pp. 85–100, Springer-Verlag, 1977.
24. F. Bookstein, *Morphometric Tools for Landmark Data: Geometry and Biology.* Cambridge University Press, 1997.
25. S. Mallat, *A Wavelet Tour of Signal Processing.* San Diego, CA: Academic Press, 1998.